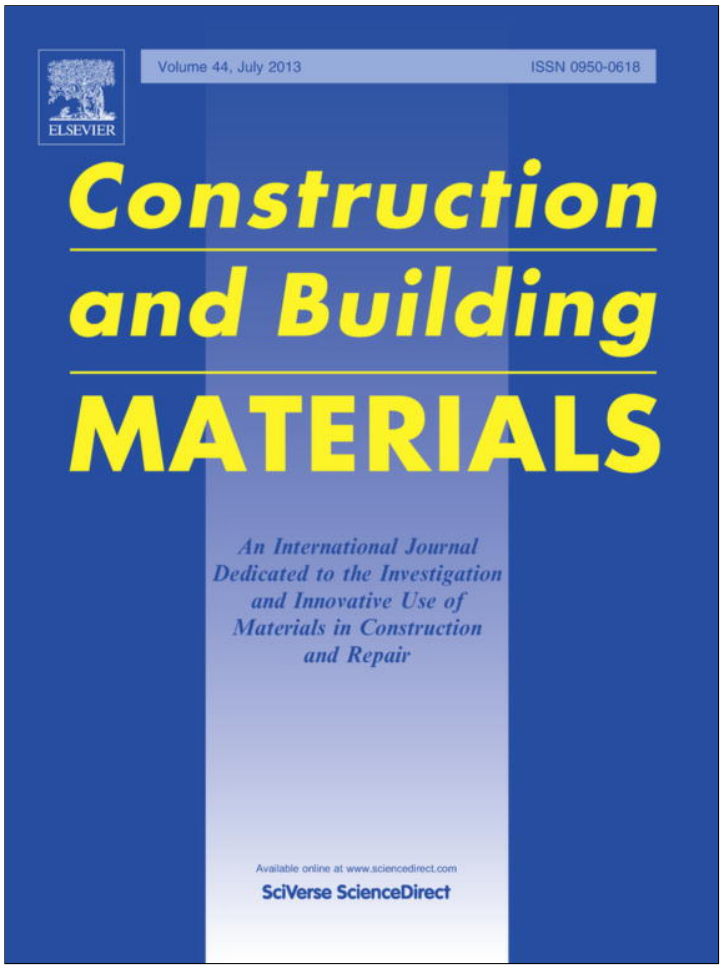

Construction and Building Materials 44 (2013) 812–821

Contents lists available at SciVerse ScienceDirect

Construction and Building Materials

journal homepage: www.elsevier.com/locate/conbuildmat

Damage evaluation of reinforced concrete beams with varying thickness using the acoustic emission technique

M.A.A. Aldahdooh, N. Muhamad Bunnori *, M.A. Megat Johari

School of Civil Engineering, Universiti Sains Malaysia (USM), Engineering Campus, Nibong Tebal 14300, Penang, Malaysia

HIGHLIGHTS

- We had studied a comparison between the visual observation and AE technique.
- We had examined the changes in the depth of beam and level of damage associated with AE parameters values.
- We had observed that by increasing the degree of damage, AE parameters values had increased except for the average frequency.
- We had observed that by increasing the beam depth, AE parameters values had increased including the average frequency.
- The severity index value increased as the depth of the beams and level of damage increased.

ARTICLE INFO

Article history:
Available online 27 December 2012

Keywords:
Acoustic emission (AE)
Damage evaluation
Reinforcement concrete
Flexural cracks

ABSTRACT

The aim of this study is to investigate the ability of the acoustic emission (AE) in order to test the effect of beam thickness on the damage mechanism of the RC beams under four-point bending. The results showed that as the level of damage increased, the values of all AE parameters increased except for average frequency; moreover, all AE parameters increased with increasing beam thickness, including the average frequency. Thus, it has been established in this work that AE can be effectively used in monitoring the behavior of RC beams with variable thickness.

1. Introduction

Reinforced concrete structures (RC) can deteriorate in service as a result of heavy loads, fatigue and aging of the structures. Cracking is commonly observed in concrete structures. It is important to understand that, the phenomenon associated with cracking can be attributed to several factors. It might result in different short term and long-term performance effects compounded by design, imposed loads, and other climatic conditions relevant to the structure [1]. In general, cracking can be broadly classified into two major categories which are micro-cracking and macro-cracking [2]. The crack development in the composite materials can be related to the mechanical interaction that exists between the inclusions such as fine sand/coarse aggregates and the cement-based matrix. This has direct bearing on the strain softening and fracture energy of the material composite structure in the cement-based matrix [3]. Such defects require monitoring to satisfy durability and serviceability requirements [2]. Structural cracks, such as flexural cracks and shear cracks, are active only if the overload condition continues or if settlement occurs [1,2]. In the regions of constant bending moment, only tensile and flexural cracks occur without sliding along the crack. Moreover, flexural crack opening is usually produced by elongation of tension reinforcing bars only when there is no slip at their end [4]. Previous study has reported that the spacing between flexural cracks is influenced by the type of longitudinal reinforcements [5,6]. Extending of structural life and avoiding structural failure can be achieved by early detection of cracks. Furthermore, the control of cracking in concrete structures is very much desirable to satisfy durability and serviceability requirements [4,7].

Nowadays, in order to detect the deterioration in concrete structure, there are several testing methods that can be adopted. Among them, the destructive testing and non-destructive testing (NDT) are very popular. These methods have distinct working principles and demonstrates different effectiveness for different types of deterioration [8].

Previous researchers have used NDT methods such as Impact-Echo method [9], Ultrasonic Pulse Velocity Method [10], Infrared Thermography [11], acoustic emission technique [12], to detect and monitor building deficiency, that requires occasional monitoring to maintain the health of building structures. Among all the NDT methods, acoustic emission (AE) is considered to be the most promising technique [13].

* Corresponding author. Tel.: +60 4 5996259; fax: +60 4 5941009.
E-mail address: cenorazura@eng.usm.my (N.M. Bunnori).

0950-0618/$ - see front matter © 2012 Elsevier Ltd. All rights reserved.
http://dx.doi.org/10.1016/j.conbuildmat.2012.11.099

There are mainly two different aspects of the AE method that distinguishes it from other NDT methods. Firstly, the energy signal originates from the sample itself making its own signal (in response to stress) in case of AE. Secondly, AE can detect dynamic process, on account of its ability to detect movement or strain, whereas most of the other methods can sense only the existing geometrical discontinuities or fractures [14]. Other advantages of AE when compared to rest of the NDT methods are: AE is applicable for local, global, remote, and continuous monitoring, whereas the rest are applicable only with respect to local scanning, less intrusive while the others are more intrusive, less geometry sensitive while the others are more geometry sensitive, material anisotropy is good with respect to AE and AE can be used in all stages of testing such as, pre-service testing, in-service testing, leak detection and location, mechanical property testing and characterization, and online monitoring [15].

In the determination of location of cracks, the principle used is the Time-of-Arrival (TOA) approach [15,16]. Microscopic and macroscopic events are two main mechanisms that generate AE, and this technique is highly sensitive for detecting active microscopic and macroscopic events in homogeneous materials or composites [17]. In addition, AE monitoring strategies can be divided into two types, namely global and local. Local monitoring tackles a specific area of damage, such as monitoring in real time damage growth in laboratory specimen [18–20], whereas global monitoring helps in evaluating the health and integrity of the entire structure [21].

AE can be defined as a localized stress wave that propagates within the materials from active deformation [15,22]. AE events also can be produced by crack onset, fiber breaks, disbands, moving dislocations, plastic deformation, and several other factors [23]. Some of the key applications of AE technology include early detection of cracking in concrete structures [24], identify damage modes in glass fiber reinforced polyester [16], prediction of fatigue crack growth in steel bridge components [25], crack classification in concrete [20,26,27], detection of cracks and disbands in aircraft composite structures [23] and global and local monitoring [21,23].

The primary objective of the AE test is to detect the presence of emission sources and to provide as many information as possible about the source [28]. There are five commonly used signal measurement parameters which are amplitude, counts, measured area under the rectified signal envelope (MARSE), duration, and rise time. Each of the AE signal feature is shown in Fig. 1.

In quantifying the damage level of any kind of structural member, the three methods commonly used in concrete structures are intensity analysis (IA), b-value, and Felicity and Calm ratio [29]. The IA method is a technique that assess the structural significance and integrity of AE data hit and the deterioration level of a structure by computing Eqs. (1) and (2), which are Historical Index (HI) and Severity Index (S_r) [21,28,30,31]. The HI is defined as a measure of the change in signal strength through the loading phase of the test, while the S_r is the average signal strength among the largest numerical values of the signal received at a sensor. Signal strength is defined mathematically as the integral of rectified voltage signal over the duration of the AE waveform packet [14]. Besides concrete structure, this method also has been successfully utilized in other structural materials such as metal and fiber-reinforced polymer (FRP) [32,33].

$$\mathrm{HI} = \frac{N}{N-K}\left(\frac{\sum_{i=K+1}^{N} S_{oi}}{\sum_{i=1}^{N} S_{oi}}\right) \tag{1}$$

$$S_r = \frac{1}{J}\left(\sum_{m=1}^{J} S_{om}\right) \tag{2}$$

where HI = Historic Index, N = Number of hits up to time t, S_{oi} = Signal strength of the ith hit, K = empirically derived constant based on material, S_r = severity index, J = empirically derived constant based on material, S_{om} = signal strength of the mth hit where the order of m is based on magnitude of the signal strength. For concrete, K and J values are related to N according to the following relations:

$$K = \begin{cases} 0, & N \le 50 \\ N-30, & 51 \le N \le 200 \\ 0.85N, & 201 \le N \le 500 \\ N-75, & N \ge 500 \end{cases}, \quad J = \begin{cases} 0, & N \le 50 \\ 50, & N > 50 \end{cases} \tag{3}$$

This technique is assessed based on the AE signal strength data collected from each sensor. The maximum values for S_r and HI are normally plotted as intensity chart as seen in Fig. 2. The chart is divided into five intensity zones, which indicate the structural significance of the emission. The descriptions for all zones are given in Table 1.

Cracking pattern and the propagation of cracks are mainly dependent on the loading type and loading conditions. According to a recent study [24], the initial cracking position depends on the internal cracks and flaws during the loading. Moreover the mechanical behavior of reinforced concrete beam can be divided into five different stages, namely; micro-cracking, first visible crack, distributed flexural cracking, shear cracking, and damage localization. During the damage localization stage the initial cracks propagated upward to the compression zone and all cracks started to localize into major cracks, causing significant widening of the width in each crack.

In this study the maximum values for S_r and HI for each level of damage are plotted on the intensity charts. The AE signal features such as rise time, average frequency, amplitude, counts, and mea-

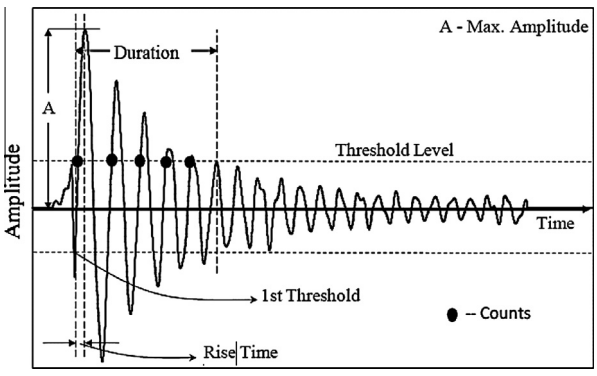

Fig. 1. Acoustic emission signal features [14,28].

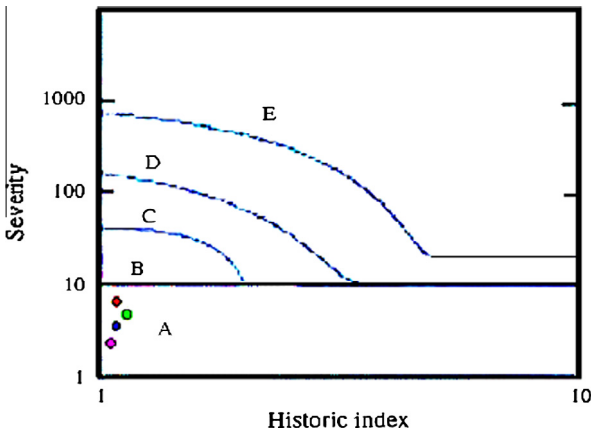

Fig. 2. Intensity analysis chart [31].

Table 1
Intensity analysis description [31].

Zone intensity	Recommended action
A	Insignificant acoustic emission
B	Note for reference in future tests. Typically minor surface defects
C	Defects require follow-up evaluation. Evaluation may be based on further data analysis or complementary destructive examination
D	Significant defect requires follow-up inspection
E	Major defect requires immediate shut-down and follow-up inspection

Table 2
Descriptions of test specimens according to ACI-08 code.

Types	Section b x h (mm)	Longitudinal reinforcement (%)	Shear reinforcement (%)	Maximum Factored load (kN)
TI	200 × 200	2Y12	R6 @ 80 mm	21.1
TII	200 × 250	2Y12	R6 @ 100 mm	27.7
TIII	200 × 300	2Y12	R6 @ 130 mm	34.3

sured duration are influenced by factors like scattering while propagating. This can be attributed to the heterogeneous structure of concrete which results from its microstructure (fine aggregate, coarse aggregates, cement, air voids, pores as well as all kinds of cracking). Moreover, the differential velocity of the distinct wave modes originating from the source crack can be one of the imperfections [27].

AE was applied to investigate the effect of aggregate size (d_{max}) on the fracture properties of high performance concrete. The results showed that, values of both, fracture energy and number of AE hits increased with increase in the aggregate size (d_{max}) [34]. This AE technique has also been applied on different volumes of concrete specimens under compression, such as cube and slenderness [35]. Studies have shown that, AE parameters are strongly influenced by factors such as type of loading and material characteristics [36–38]. However, in spite of its several applications, there is still lack of work investigating the effect of size of structure on the AE output data. In the present study, the AE results of bending tests involving different types of RC beams are presented and discussed. Twelve specimens of RC beams with different thickness are prepared and tested under four point bending, with associated monitoring of their AE activity.

The objective of the present study is to investigate the capability of AE technique for monitoring of RC beams subjected to flexural failure mode by considering various beam thicknesses. Moreover, the structural integrity and quantification of the degree of deterioration at each stage of the mechanical behavior of reinforced concrete beams during loading until failure are carried out using the IA method.

Table 3
Properties of concrete and steel reinforcement.

Materials	Concrete	Steel
Compressive strength (MPa)	47	–
Yield stress (MPa)	–	420

2. Experimental program

2.1. Sample preparation

Three types of RC beams with same span length 1500 mm but different thicknesses were prepared and the dimensions are presented in Table 2. In this study, the beams were reinforced with 2Y10 and 2R8 diameter deformed steel bars at the tension and compression faces respectively, according to American Standard (ACI318-08). They were denoted by Type I (TI), Type II (TII) and, Type III (TIII) with stirrups center-to-center spacing of R6 diameter at 80 mm, 100 mm and 130 mm, respectively. The cross section detailing for all types are presented in Fig. 3.

2.2. Properties of materials

The specified characteristic compressive concrete strength is 45 MPa while the compressive concrete strength on the day of testing was 47 MPa. The mechanical properties of concrete and steel are given in Table 3. All RC beams were cured in water for 28 days prior to testing.

2.3. Loading and acoustic emission system

All the beams were tested under four point loading (stepwise monotonic loading) to examine the flexural cracks behavior and the level of damage in all specimens using the AE technique, as shown in Fig. 4. The tests were conducted using a 500 kN capacity loading frame system consisting of a hydraulic jack, load cell (TCIP-20B) and a Kyowa data logger (UCAM-20PC)). Four AE sensors (R6I) manufactured by Physical Acoustics Corporation (PAC) with frequency ranges of 35–100 kHz were mounted on the specimen surface using magnetic clamp. Silicon grease was used as coupling agent between the sensor and the concrete surface. The locations of the four sensors (S1–S4) are shown in Fig. 4. Moreover, the symbols (H and W) represent respectively the thickness and the width of the beam, as shown in Fig. 4.

AE source locations were identified by the AE detection system (MICRO – SAMOS (μSAMOS) Digital AE System) based on the differences in AE signals arrival time at an array of four AE sensors on the specimen and a preset wave velocity measured with pencil lead breaks in accordance with Hsu–Nielsen source method [39].

In this study, the sampling rate was set to '1000kSPS' and the pre trigger setting were 250.000 μs, hit definition time (HDT) was 2000 μs, Wave velocity was 3500 m/s and lockout time (HLT) was 500 μs. To eliminate electrical and mechanical noises, the threshold level was set at 45 dB. The load was applied slowly on the beam until 0.5 kN to ensure that the two point load is in contact with the beam surface, with the same moment the monitoring system was hold for 1 min for ensuring there is no noise of emission detected during that period. Firstly, the load is applied slowly on the beam until 0.5 kN so that the two point load is in contact with the beam's surface. After a minute, the load was applied in stepwise loading as presented in Fig. 5. The first step of loading was from 0.5 to 10 kN and it was kept constant for 3 min prior to the next loading step until the failure stage.

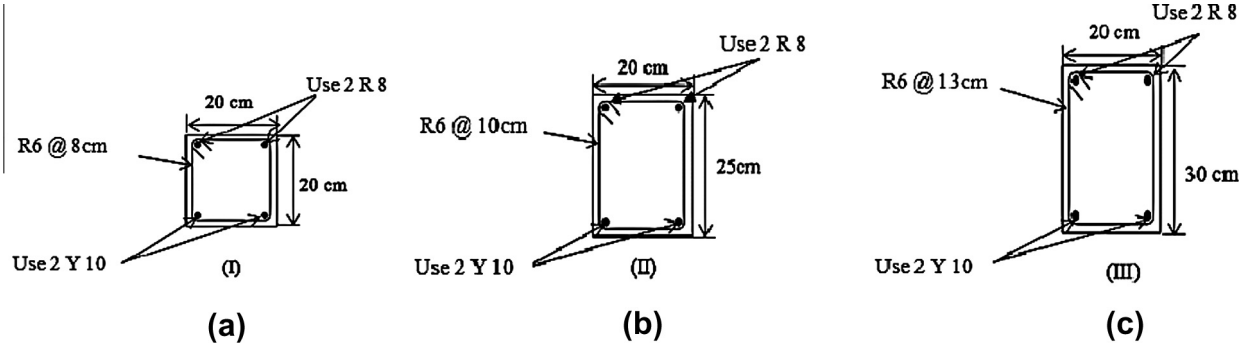

Fig. 3. Cross section detailing for beams: (a) Type I, (b) Type II, and (c) Type III.

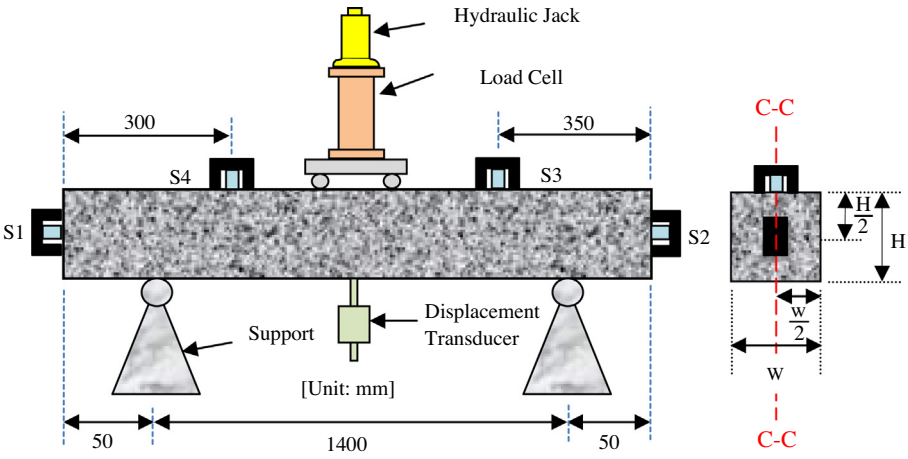

Fig. 4. Set-up of the four point bending test.

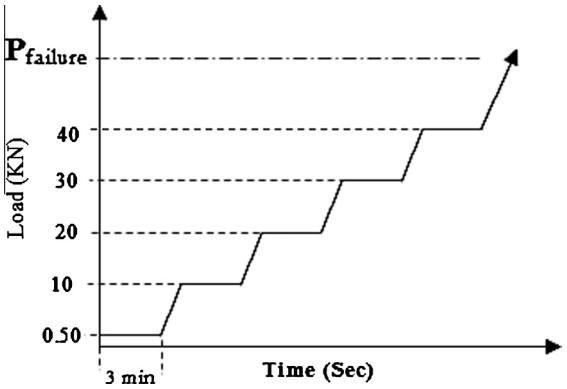

Fig. 5. Graphical representation of the stepwise loading.

3. Test results and discussion

The test results and the subsequent discussion focused on all stages of damage, while the important region was the region between level of damage I and level of damage II, where the micro-cracking and the onset of surface cracking usually occurred, respectively as shown in Fig. 6.

3.1. Crack development

The crack pattern and propagation are mainly dependent on the loading type and loading conditions. In the most types of RC structure when load is applied until failure; shear cracks developed after the formation of the tensile cracks. The formations of the tensile cracks are developed at the earlier stages of loading [27,40]. The initial cracking position depends on the internal cracks and flaws during loading. Hence, the propagation of internal cracks will lead to the first visual crack [24,41]. From the test and observation, it was found that all beams failed in flexural mode. Fig. 6 shows the load–deflection curve for the three types of RC beams, and the different damage levels, namely (I) Micro-cracking, (II) First visible cracks (point A), (III) distributed flexural (point B), and (IV) Damage localization (point C) are clearly identified on the load–deflection curves. Fig. 6d shows the load and the corresponding displacement curve of one beam for each type TI, TII and TIII, where these beams have been selected to represent their particular group.

Type I beams, which has the smallest thickness are regarded as control beams. Fig. 7a–e, shows the typical crack propagation process observed for one of the control beams (TI) at the specified damage levels, while Fig. 8a and b shows the crack patterns obtained through visual observation for the TII and TIII beams, respectively at the identified damage levels. In Figs. 7 and 8 the numbered tick marks along the length of the cracks are referred to the load values in kN.

From the test and observation, it was found that all beams failed in flexural mode as shown in Fig. 7. Determination of the failure stages of the reinforced concrete beams was done based on visual observation of the onset of crack; as shown in Fig. 7b–e. While, in Fig. 7a visible cracks were not appearing at the outer surface of the concrete beams, however micro-cracks are developed inside the RC beams, which can be detected by using the AE technique. In this paper the acoustic emission technique was used for determining the onset and growth of internal micro-cracking.

In the controlled beam the first cracks was observed visually on the surface at approximately 930 mm in Fig. 7b at 15 kN (point A) as shown in Fig. 6a. While the first cracks for TII and TIII beams at 23 kN and 36 kN (at point A as seen in Fig. 6b and c) were observed at approximately 510 mm, 700 mm, 820 mm, and 1000 mm (refer Fig. 8a), 480 mm and 715 mm (refer Fig. 8b) respectively. Some of these cracks occurred at the same time, but all of these cracks occurred at the same stage before reaching point (A) as shown in Fig. 6. The respective load corresponding to the first crack for beams TII and TIII is shown in Fig. 6b and c, respectively.

The crack propagation in TII and TIII were largely spread in a limited area between the two points of load. Moreover, it can be noticed from Fig. 7 that, TI has similar pattern of crack propagation under load. For TI, as the load increased, flexural cracks propagated and positioned between the two point loads of the beam after an initial flexural crack was generated at the bottom surface of the mid span in the tension zone. These flexural cracks were observed at approximately 460 mm, 585 mm, 760 mm, 910 mm and 1070 mm (refer Fig. 7c) at 28 kN (point B depicted in Fig. 6a). While for TII and TIII, these were observed at an applied load of 37 kN and 48 kN, respectively depicted in Fig 6b and c.

As the load was further increased, the initial cracks propagated upward to the compression zone and all cracks started to localize into major cracks where the width of each crack was significantly widened, which correspond to damage localization stage. These cracks were observed at approximately 460 mm, 585 mm, 760 mm, 910 mm and 1070 mm (refer Fig. 7d) at 60 kN (point C) depicted in Fig. 6a. While for TII and TIII, these were observed at an applied load of 97 kN and 120 kN (point C) respectively, as shown in Fig 6b and c.

The cracks start to localize at an applied load of 60 kN, 85 kN and 107 kN (point C)for TI, TII and TIII beam, as shown in Fig 6a–c, respectively.

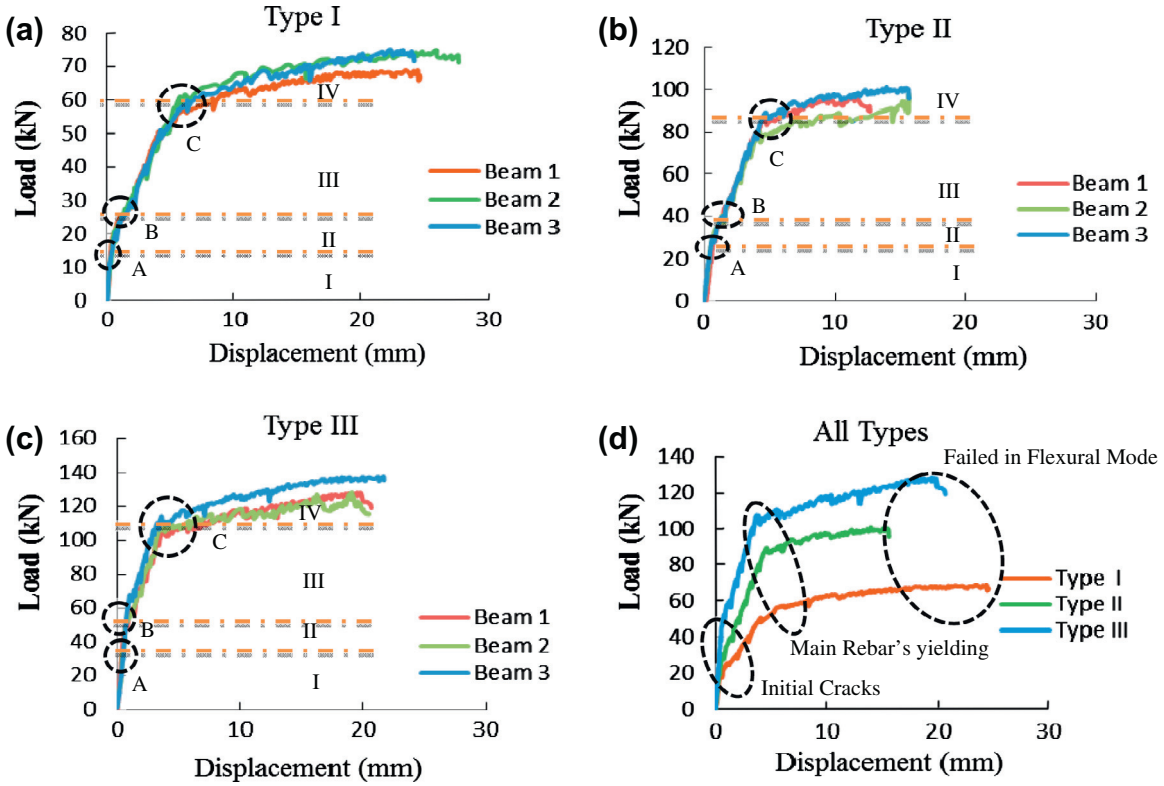

Fig. 6. Load–displacement: (a) Type I, (b) Type II, (c) Type III and, (d) All Types.

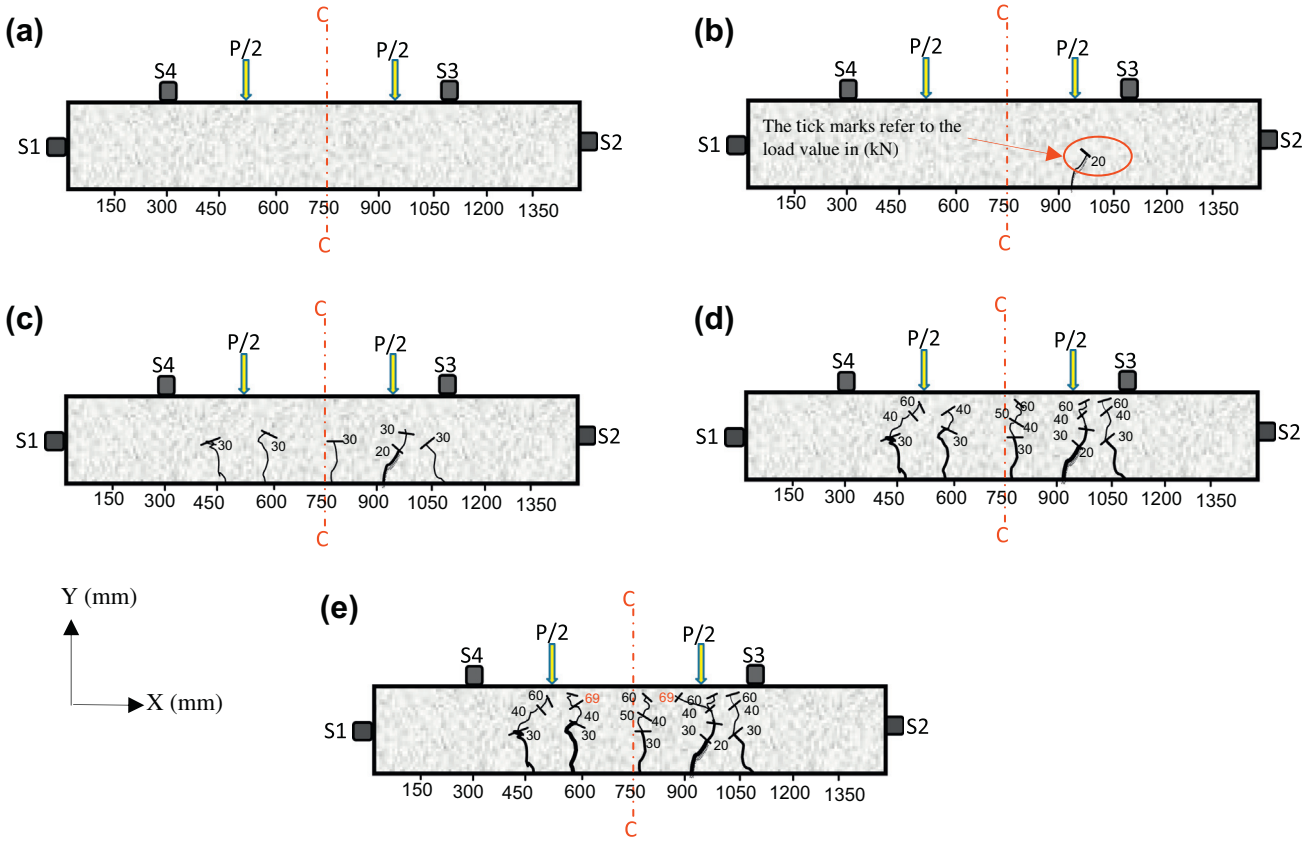

Fig. 7. Crack patterns obtained by visual observation of control beam TI at each stage of damage: (a) stage I – as a micro-cracking, (b) stage II – as a first visible cracks, (c) stage III – as a distributed flexural cracks, (d) stage IV – as damage localization, (e) failure mode. (Load in kN, and distance in mm).

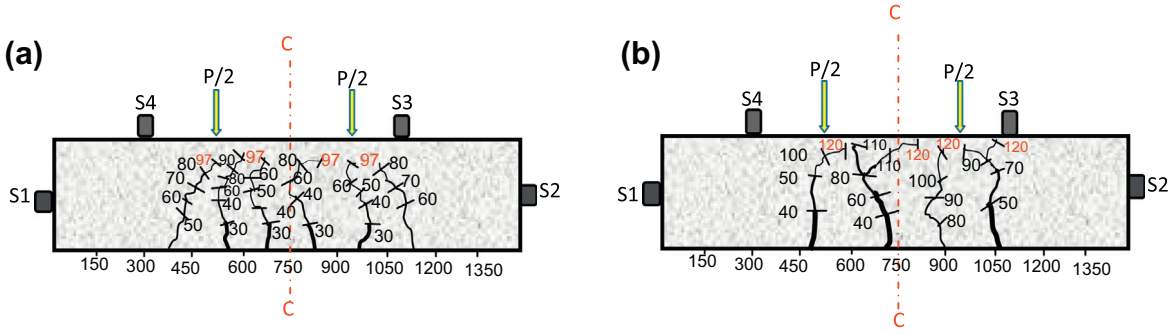

Fig. 8. Crack patterns obtained by visual observation at the final stage of damage : (a) TII, (b) TIII. (Load in kN, and distance in mm).

When the load reached the maximum capacity of 69 kN, 97 kN, and 120 kN for TI, TII, and TIII beams respectively (Fig. 6d), the beams failed in conventional ductile flexure with the yielding of the tension steel, followed by the crushing of the concrete in the compression zone. Finally, it can be concluded that the overall crack distributions for all beams were similar to that of the TI beam.

3.2. Characteristics of AE parameters

The characteristics of the AE parameter from the AE signals of TI, TII, and TIII beams are shown in Fig. 9. The AE signals for all beams were divided into four levels of damage, according to damage stages specified in Section 3.1. It is to be noted that, for each damage level, 100 representative points were plotted for each AE parameter. These 100 point were obtained by dividing the AE signals for each beam into four levels according to their level of damage. Again, these AE parameter values for each level of damage were further divided into 100 intervals and the average of the AE parameter values were determined for each interval. The trend lines shown in Fig. 9 was fitted to the AE data output in order to validate the trend of the AE counts number, duration values and average frequency values at each level of damage, particularly for the first level of damage (I) and at the damage localization level (IV). The characteristics of the AE parameter at the different stages of damage are presented in Table 4. These include the AE elastic wave with average amplitude above 45 dB at different damage levels of the TI, TII, and TIII beams, duration, frequency, counts, absolute energy, etc.

The test results and the subsequent discussion focused on all stages of damage, whereas the important region was the region between stage I and II, where the micro-cracking and the onset of surface cracking usually occurred. Based on the comparison between visual observation and the AE results for the three types of beams as described in Table 4, it is found that the minimum of the cumulative absolute energy at onset of the first crack should exceed 1.63×10^6 (aJ), 1.4×10^7 (aJ), and 1.85×10^7 (aJ), for thicknesses 20, 25, and 30 cm, respectively. Moreover, when the specimens experienced localization of damage, the absolute energy will increase dramatically by approximately five to seven times.

Fig. 9A shows the relationship between the count and the amplitude, on account of the damages incurred by TI, TII, and TIII beams. It is clear that increasing the beam thickness results in slight increase of amplitude; however this increase is minor. This may be due to the fact that all beams failed in the same manner by flexural mode. With regards to the counts number, it is obvious that the counts range and its maximum value for each damage level increases with the increase in beam thickness. Likewise the maximum difference between damage level increases as beam thickness increases. In general, all beams, count increases with the evolution of damage up to ultimate load [41].

Fig. 9B shows plots of duration versus amplitude from AE signals for the TI, TII and TIII beams. The trend of duration is almost similar to the trend of counts reported by previous researchers [41]. In the case of TI, the duration was found to be less than 1000 μs until the first crack appeared and reflected on the surface of the beam. Whereas for, TII and TIII it was observed to be less than 1800 μs and 2000 μs respectively. The distribution of duration varied between 500 μs and 3200 μs when the damage level III and IV were reported for the first type of beams TI. However, for types TII and TIII the duration was widely distributed between 500 μs–4000 μs and 800 μs–5000 μs, respectively.

Fig. 9C shows the relationship between the average frequency and amplitude for AE signals representing the TI, TII and TIII beams. It can be inferred from Fig. 9C that the highest value of average frequency is always associated with the first level of damage. Moreover, the average frequency values at the first level of damage are higher than the average frequency values at the next stage. It is observed that the AE signals at the earlier damage stage, such as the micro- cracking stage for TI were in the range of 75–175 kHz, while for TII and TIII were in the range of 75–200 kHz and 75–300 kHz, respectively as shown in Fig. 9C. When the damage level III and IV were achieved in the first type of beams TI, the average frequency was in the range of 50–105 kHz. Whereas for the others types, TII and TIII, the average frequency were widely distributed between 50–150 kHz and 50–175 kHz, respectively. This behavior is similar to that observed by several other researchers [20,27,36,42] and reported that the flexural cracks developed usually at the initial stages of loading. Hence, the average frequency is one of the sensitive signal features of AE which can be affected by the failure modes (shear or flexural mode). Moreover, the value of this average frequency in the tensile mode crack is always higher than its value in the shear mode crack.

The visual observations confirmed that the development of crack at each level of damage as specified in Section 3.1. Thus these results clearly show that the failure occurred by the majority of flexure cracks for all beams at all levels of damage as depicted in Figs. 7 and 8.

It was observed that the average frequency value at the initial stages of damage was high due to flexural cracks. Moreover, the average frequency at the earlier level of damage (micro-cracking stage) is higher than the average frequency at later level of damage (localized crack stage) [20,27,36]. Generally, at the later stages of damage the AE hit rate is lower than the previous stage having decreasing tendency. This phenomenon can be attributed to the reduction in the cross sectional area of the beam which increases the damage level to the point of ultimate failure [27].

On the other hand it is also noticed from Fig. 9C and Table 4 that as beam thickness increases average frequency increases for all damage levels. This is because, as the beam thickness increases the crack length decreases, which in turn results in the increase in its frequency. This observation corroborates the fact that reduc-

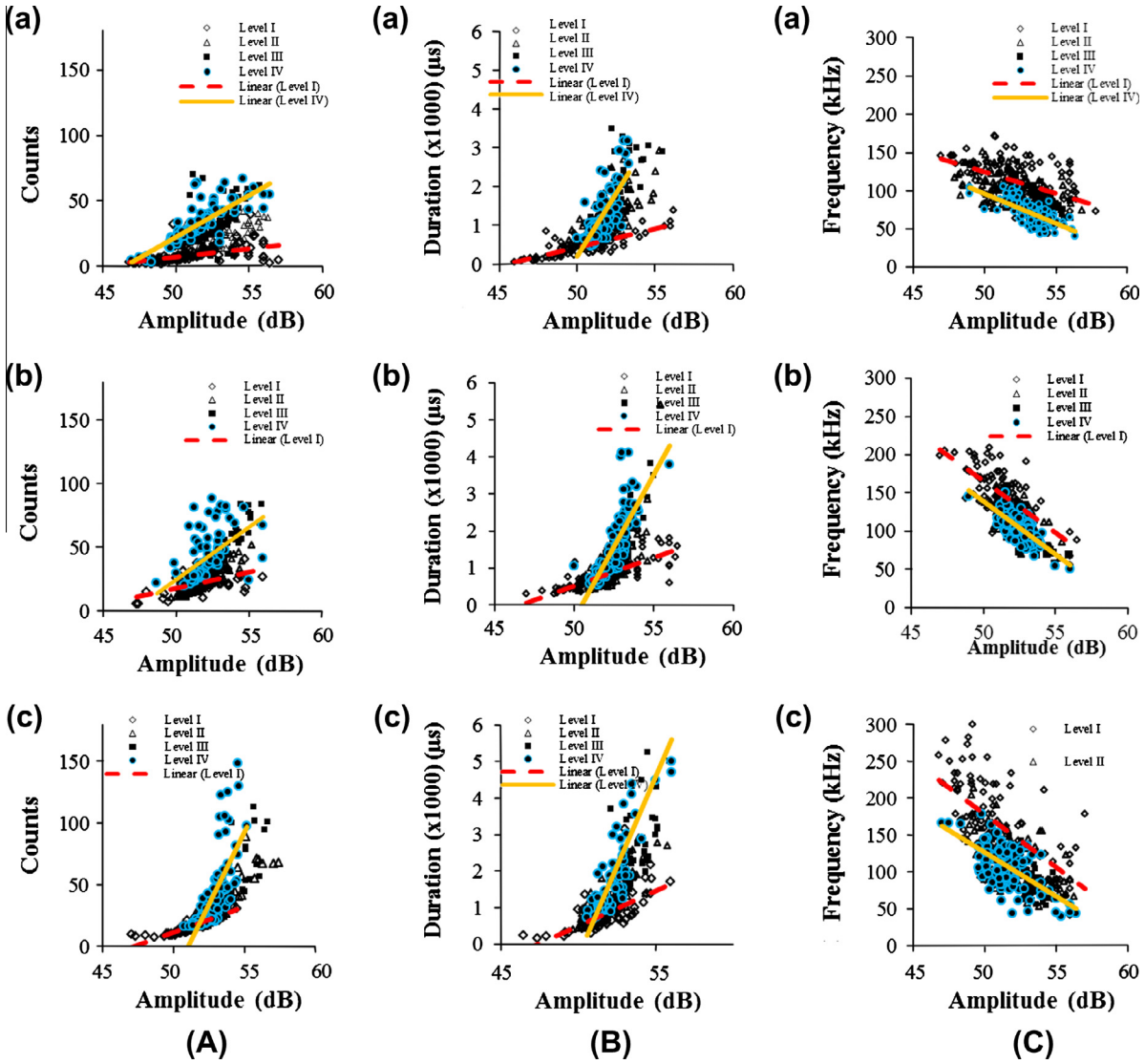

Fig. 9. (A) Typical AE counts versus amplitude: (a) TI beams; (b) TII beams and (c) TIII beams; (B) Typical AE duration time versus amplitude: (a) TI beams; (b) TII beams and (c) TIII beams; (C) Typical AE frequency versus amplitude: (a) TI beams; (b) TII beams and (c) TIII beams.

Table 4
Characteristics of AE parameters.

Types	Level of damage	Duration[a] (×1000 μs)	AMP (dB)[a]	FRQ (kHz)[a]	ABS-energy (aJ)[c]	Hits[b]	% of total hits	Counts[b]
TI								
	I	0.905	47.83	102	4.95E+05	440	0.65	21,235
	II	0.976	51.50	104	1.63E+06	2889	4.28	81,422
	III	1.977	52.20	87	7.35E+07	35,014	51.93	968,137
	IV	1.392	51.65	87	8.87E+07	29,082	43.13	998,813
TII								
	I	0.824	51.33	127	7.60E+05	7,656	5.46	24,700
	II	1.473	52.40	102	1.40E+07	14,366	10.24	83,859
	III	1.732	52.75	104	1.26E+08	60,750	43.30	1,091,859
	IV	1.409	52.49	103	2.34E+08	57,512	41.00	1,100,704
TIII								
	I	0.9622	51.70	146	1.78E+06	2791	2.06	25,118
	II	2.094	52.22	108	1.85E+07	14,235	10.50	435,615
	III	2.769	53.00	103	1.59E+08	67,228	49.57	1,105,529
	IV	1.449	52.22	114	3.77E+08	64,007	47.19	1,110,590

[a] Duration, amplitude, and frequency are average values at the each level of damage.
[b] Number of count and hits are accumulative values at each level of damage.
[c] Absolute energy is the maximum average values at each level of damage.

tion in the cross sectional area of the beam increases the damage level to the point of ultimate failure [27]. This also means that, the crack length obtained by the application of a load having same magnitude on the three beams TI, TII and TIII, the shortest crack length will be associated with largest beam thickness. This shows that the reduction in the cross sectional area of the beam will decrease as beam thickness increases as indicated in Figs. 7 and 8. Furthermore, the lowest reduction will be associated with largest beam thickness, which in this case is the third type (TIII). Therefore, AE hit rate in the smallest thickness will be lower than the largest thickness at each level.

These observations are comparable with the shear cracks phenomena, in which the shear crack (diagonal cracks) lengths, are always longer than the flexural crack (vertical cracks) length. This behavior can be related to AE waveform shape. Kumar [42] has reported that the waveform shape is one of the most sensitive characteristic of the fracture mode. Therefore, the value of the rise time parameter in the tensile mode crack is shorter and the average frequency value is higher. Whilst the shear mode crack results in longer waveforms, having longer rise time and lower average frequency [20,27,36]. This is mainly due to the transmitted energy quantity and speed, wherein inverse relationship exists between the energy quantity and speed. Hence, the speed of energy at the later levels of damage (mix-mode cracks) is always slower than the earlier levels of damage (pure flexural cracks). This is due to the fact that larger part of energy is transferred in the shear waveform. Therefore, the maximum peak of the waveform delays considerably when compared to the onset of the initial longitudinal arrivals [27].

In Table 4, it can be seen that the maximum duration, amplitude, and hits are always occurring at damage level III. This result could be explained by the characteristics of AE signals caused by the debonding between the reinforcement and the concrete, and also due to the initiation of crack localization and main rebar yielding as shown in Fig. 6d [41].

4. Damage quantification

The data has been quantified using the IA technique which entails the accumulation of AE data gained from the successive stepwise loading. The AE data was used to determine the indices given in Eqs. (1) and (2). Moreover, intensity chart is produced by plotting the maximum of the average values of the HI and S_r as shown in Fig. 10. In this regard, the intensity chart is divided into five intensity zones (I–V) which identify the structural significance of a given sequence of AE events as previously described and summarized in Table 1 [28,43]. Where, each zone is related to a different level of damage (Fig. 6); for example zone I is related to level of damage I, zone II is related to level of damage II, until it reaches damage level IV. However, the IA indices values for zone V were determined after the complete failure of the beams. This stage is called as failure mode stage (V) as can be seen from Figs. 7e, 10e, 11 and 12.

Generally, intensity values clustered towards the top are associated with phenomena of high structural significance, whereas less structurally significant events concentrate near the bottom as shown in Fig. 11. Throughout this research, the intensity chart was established for all given AE sensor intensity values of high structural significance. However, only the results obtained from sensor no. 3 and no. 4 were used in plotting the intensity chart because it nearby the damage location and the remaining sensor data were avoided due to presence of noise.

Fig. 10a shows the intensity charts for TI at stage I (micro-cracking), where no follow-up is recommended due to insignificant acoustic emission. The value for sensor 4 is below and left of the value for sensor 3, which is due to the micro-cracking that had started within the stage I before the first visual crack was observed. Therefore, these microcracks are invisible in Fig. 7a, and can only be detected and quantified by the AE system as shown Fig. 10a.

After the first stage, the increase in severity index value is more in channel 3 which was closer to the area of first visible cracking corresponding to stage II as shown in Fig. 10b where the level of damage is categorized as minor surface defects which require attention in future tests. In fact, the value of the severity index from sensor 4 is slightly lower at the left corner compared to the value of sensor 3; this confirms that the slightly greater amount of minor damage occurred in the area that is closer to sensor 3 as shown in Fig. 7b.

Fig. 10c shows the intensity charts at stage III (distributed flexural and shear cracks), where follow up evaluation of the defects is required. Since the value of sensor 3 is slightly higher than sensor 4, such result confirms that slightly greater amount of intermedi-

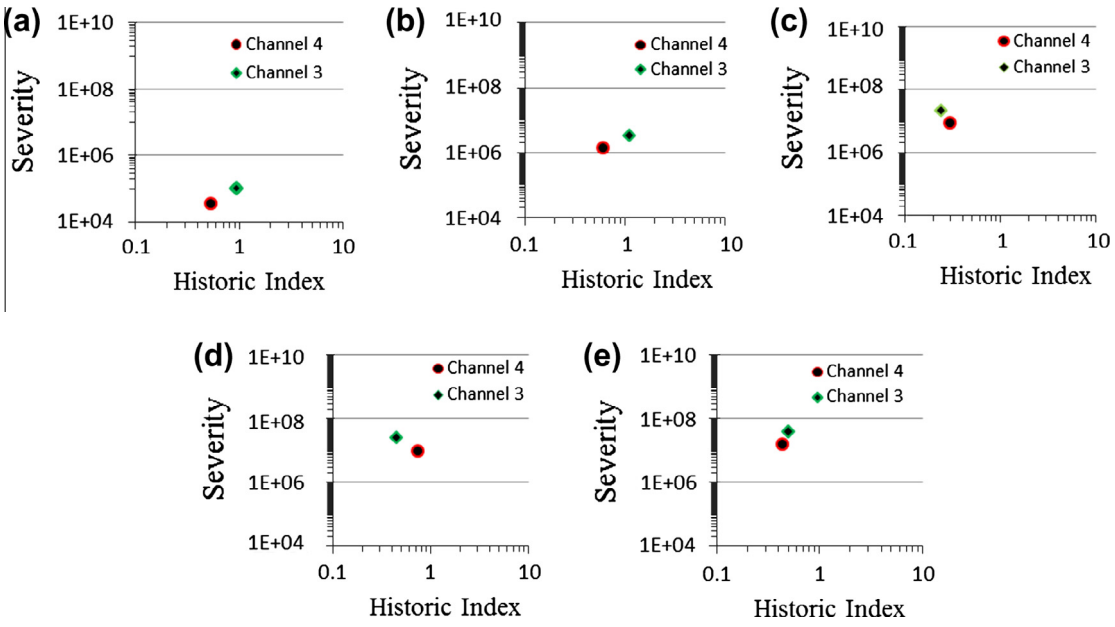

Fig. 10. Intensity charts for category I at each stage: (a) stage I, (b) stage II (c) stage III, (d) stage IV, and (e) failure stage V.

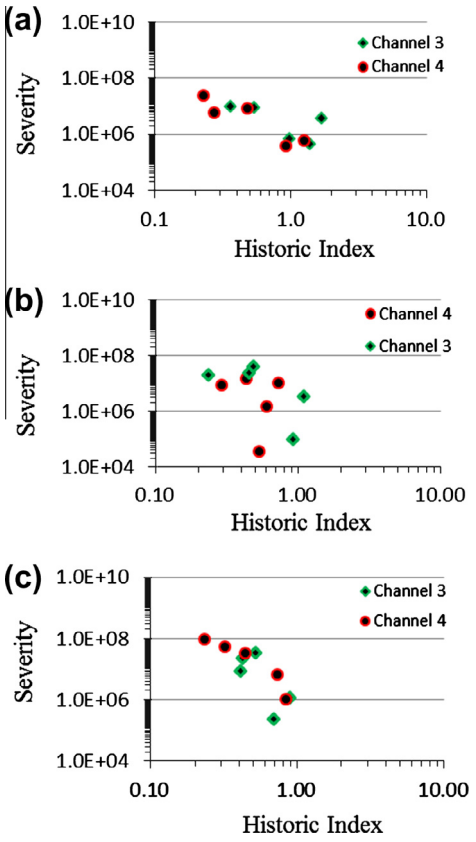

Fig. 11. Intensity charts for all stages: (a) TI, (b) TII, and (c) TIII.

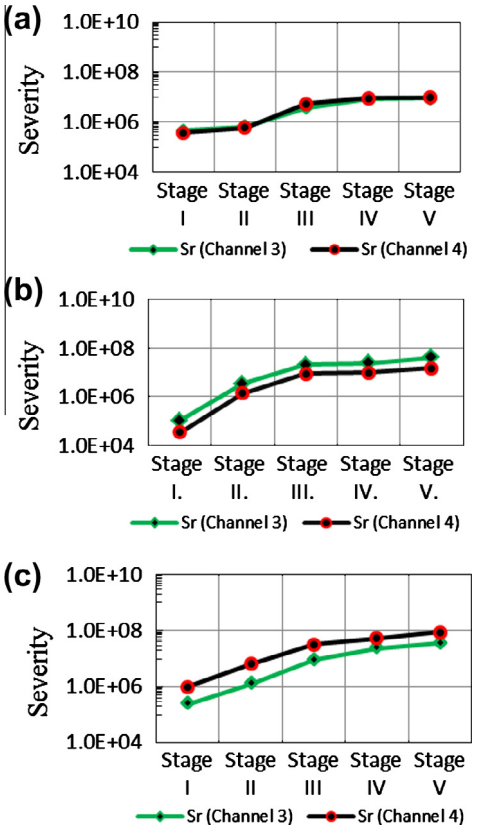

Fig. 12. Severity index as a function of damage level for all stages: (a) TI, (b) TII, and (c) TIII.

ate surface defects occurred in area closer to sensor 3, and this fact is confirmed in Fig. 7c.

After stage III, all the cracks begin to localize into major cracks where the width of each crack, widened and increased significantly. This stage is known as the damage localization stage as can be inferred from Fig. 7d. In this stage the recommended action is significant defect requiring follow-up inspection. During damage localization the value of severity index from sensor 3 and the value from sensor 4 are almost the same as shown in Fig. 10d, which means that the amount of significant defects occurred in middle of the beam which is between sensor 3 and sensor 4 as indicated in Fig. 7d.

Finally at failure stage the recommended action is major defect that requires immediate shut-down and follow-up inspection. Moreover, Fig. 10e shows that the severity index value from sensor 3 is slightly higher than the value of sensor 4, with slightly different HI value. This confirms that the failure occurred at the middle of the beam in flexural mode.

Figs. 11 and 12 summarize the intensity charts and severity index, respectively for all stages for TI, TII, and TIII. Globally, these figures show that the pattern of intensity charts analysis is quite similar between each other. This indicates the process of the damage mechanism commencing from micro-cracking stage till the end of failure stage as presented in the chart for each sensor. According to the chart, the high structure values for intensity analysis were plotted towards the top of the chart, while the values of less significant are in the bottom area.

From Figs. 11a–c and 12a–c, it could be observed that TIII had the highest value of the severity index at all levels (i.e., stage I – failure stage) of damage. This indicates that the severity index value in the three types tend to increase with the increase in the thickness of the beams (i.e., 200–300 mm); and also by increasing the level of damage. Based on the results from the intensity charts, the application promises to provide quantitative information regarding the identification of damage areas and its ability to classify the different sources of damage.

5. Conclusions

Based on the AE signal strength analysis and the intensity analysis presented in this paper, the following conclusions could be made:

(1) From the observation for all concrete beams, it was found that there were four stages of mechanical behavior the long beam would experience before failure. These four stages are micro-cracking, localized crack propagation, distributed flexural cracking and finally the damage localization.
(2) Based on comparison between visual observation and the AE results for the three types of beams, it is found that at the onset of the first visible crack, the minimum of the cumulative absolute energy should exceed 1.63×10^6 (aJ), 1.4×10^7 (aJ), and 1.85×10^7 (aJ), for thicknesses 20, 25, and 30 cm, respectively. Moreover, when the specimens experienced localization of damage, the absolute energy will increase dramatically by approximately about five to seven times.
(3) As the level of damage increases, values of duration, number of counts, cumulative absolute energy, number of hits, and amplitude increase. The increase in rate differs from one AE parameter to another; amplitude having the smallest rate. Frequency also varies and it decreases as level of damage increases.
(4) The effects of beam thickness on all AE parameters are almost the same. The average and cumulative values of these parameters increase with increasing in the beam thickness.

(5) The severity index value increases as the thickness of the beams and level of damage increases.

In general, it can be fairly concluded that AE is a promising technique to monitor and detect the location of the cracks.

Acknowledgments

The authors wish to acknowledge Universiti Sains Malaysia (USM) for providing the financial support through the USM fellowship scheme, and Short Term Grand (304/PAWAM/6039047).

References

[1] Yoon DJ, Weiss WJ, Shah SP. Assessing damage in corroded reinforced concrete using acoustic emission. J Eng Mech 2000;126(3):273–83.
[2] Kabir S, Rivard P, He DC, Thivierge P. Damage assessment for concrete structure using image processing techniques on acoustic borehole imagery. Constr Build Mater 2009;23(10):3166–74.
[3] Wittmann F. Crack formation and fracture energy of normal and high strength concrete. Sadhana 2002;27(4):413–23.
[4] Hassan HM, Farghaly SA, Ueda T. Displacement at shear crack in beams with shear reinforcement under static and fatigue loading. Jpn Soc Civil Eng JSCE 1991;15(433):215–22.
[5] Hassan HM, Ueda T. Relative displacement along shear crack of reinforced concrete beam. Proc JCI 1987;9(2):699–704.
[6] Zararis PD. Shear strength and minimum shear reinforcement of reinforced concrete slender beams. ACI Struct J 2003;100(2).
[7] Wan KT, Leung CKY. Fiber optic sensor for the monitoring of mixed mode cracks in structures. Sensors Actuat A 2007;135(2):370–80.
[8] Mahmood A. Structural health monitoring using non destructive testing of concrete [bachelor thesis]. Rourkela, Odisha: National Institute of Technology; 2008.
[9] Sansalone M, Carino NJ. Detecting delaminations in concrete slabs with and without overlays using the impact-echo method. ACI Mater J 1989;86(2):175–84.
[10] Abo-Qudais SA. Effect of concrete mixing parameters on propagation of ultrasonic waves. Constr Build Mater 2005;19(4):257–63.
[11] Barreira E, de Freitas VP. Evaluation of building materials using infrared thermography. Constr Build Mater 2007;21(1):218–24.
[12] Reinhardt H, Grosse C. Continuous monitoring of setting and hardening of mortar and concrete. Constr Build Mater 2004;18(3):145–54.
[13] Matsuyama K, Yamada M, Ohtsu M. On-site measurement of delamination and surface crack in concrete structure by visualized NDT. Constr Build Mater 2010;24(12):2381–7.
[14] Degala S. Acoustic emission monitoring of reinforced concrete systems retrofitted with CFRP [master's thesis]. University of Pittsburgh; 2008.
[15] Miller RK, McIntire P. Nondestructive Testing Handbook. vol. 5. Acoustic Emission Testing. American Society for Nondestructive Testing; 1987. p. 603.
[16] Huguet S, Godin N, Gaertner R, Salmon L, Villard D. Use of acoustic emission to identify damage modes in glass fibre reinforced polyester. Compos Sci Technol 2002;62(10–11):1433–44.
[17] Luo X, Haya H, Inaba T, Shiotani T, Nakanishi Y. Damage evaluation of railway structures by using train-induced AE. Constr Build Mater 2004;18(3):215–23.
[18] Vidya Sagar R, Raghu Prasad B. An experimental study on acoustic emission energy as a quantitative measure of size independent specific fracture energy of concrete beams. Constr Build Mater 2011;25(5):2349–57.
[19] Shah SG, Chandra Kishen J. Fracture behavior of concrete–concrete interface using acoustic emission technique. Eng Fract Mech 2010;77(6):908–24.
[20] Ohno K, Ohtsu M. Crack classification in concrete based on acoustic emission. Constr Build Mater 2010;24(12):2339–46.
[21] Nair A, Cai C. Acoustic emission monitoring of bridges: review and case studies. Eng Struct 2010;32(6):1704–14.
[22] Drouillard T. A history of acoustic emission. J Acoust Emission 1996;14(1):1–34.
[23] Zook JD, Burns DW, Schoess JN, Guckel H. Optically resonant microbeams. P Soc Photo – Opt Ins 1995;2383:6–16.
[24] Bunnori NM, Lark RJ, Holford KM. The use of acoustic emission for the early detection of cracking in concrete structures. Mag Concr Res 2011;63(9):683–8.
[25] Yu JG, Ziehl P, Zarate B, Caicedo J. Prediction of fatigue crack growth in steel bridge components using acoustic emission. J Constr Steel Res 2011;67(8):1254–60.
[26] Grosse C, Reinhardt H, Dahm T. Localization and classification of fracture types in concrete with quantitative acoustic emission measurement techniques. NDT and E Int 1997;30(4):223–30.
[27] Aggelis DG. Classification of cracking mode in concrete by acoustic emission parameters. Mech Res Commun 2011;38(3):153–7.
[28] Degala S, Rizzo P, Ramanathan K, Harries KA. Acoustic emission monitoring of CFRP reinforced concrete slabs. Constr Build Mater 2009;23(5):2016–26.
[29] Lovejoy SC. Acoustic emission testing of beams to simulate shm of vintage reinforced concrete deck girder highway bridges. Struct Health Monit 2008;7(4):329.
[30] Proverbio E. Evaluation of deterioration in reinforced concrete structures by AE technique. Mater Corros 2011;62(2):161–9.
[31] Golaski L, Gebski P, Ono K. Diagnostics of reinforced concrete bridges by acoustic emission. J Acoust Emission 2002;20(2002):83–9.
[32] Shahidan S, Bunnori NM, Md Nor N, Basri SR. Damage severity evaluation on reinforced concrete beam by means of acoustic emission signal and intensity analysis. In: IEEE symposium on industrial electronics & applications (ISIEA 2011). Langkawi Island, Malaysia; 2011. p. 357–61.
[33] Nair A, Cai CS. Acoustic emission monitoring of bridges: review and case studies. Eng Struct 2010;32(6):1704–14.
[34] Chen B, Liu J. Investigation of effects of aggregate size on the fracture behavior of high performance concrete by acoustic emission. Constr Build Mater 2007;21(8):1696–701.
[35] Carpinteri A, Lacidogna G, Pugno N. Structural damage diagnosis and life-time assessment by acoustic emission monitoring. Eng Fract Mech 2007;74(1):273–89.
[36] Soulioti D, Barkoula N, Paipetis A, Matikas T, Shiotani T, Aggelis D. Acoustic emission behavior of steel fibre reinforced concrete under bending. Constr Build Mater 2009;23(12):3532–6.
[37] Aggelis D, Soulioti D, Barkoula N, Paipetis A, Matikas T. Influence of fiber chemical coating on the acoustic emission behavior of steel fiber reinforced concrete. Cem Concr Compos 2011;34(1):62–7.
[38] Chen B, Liu J. Damage in carbon fiber-reinforced concrete, monitored by both electrical resistance measurement and acoustic emission analysis. Constr Build Mater 2008;22(11):2196–201.
[39] ASTME976. Standard Guide for determining the reproducibility of acoustic emission sensor response. The American Society for Testing and Materials; 2010.
[40] Yuyama S, Li Z, Ito Y, Arazoe M. Quantitative analysis of fracture process in RC column foundation by moment tensor analysis of acoustic emission. Constr Build Mater 1999;13(1–2):87–97.
[41] Yun HD, Choi WC, Seo SY. Acoustic emission activities and damage evaluation of reinforced concrete beams strengthened with CFRP sheets. NDT and E Int 2010;43(7):615–28.
[42] Kumar A, Gupta A. Acoustic emission in fiber reinforced concrete. Exp Mech 1996;36(3):258–61.
[43] Golaski L, Gebski Pawel, Kanji O. Diagnostic of reinforced concrete bridge by acoustic emission. J Acoust Emission 2002; 20.